THE GEOLOGICAL SOCIETY OF AMERICA®

Strontium and carbon isotopic evidence for decoupling of pCO_2 from continental weathering at the apex of the late Paleozoic glaciation

Jitao Chen[1,2,3]*, Isabel P. Montañez[1], Yuping Qi[2,3], Shuzhong Shen[2,4], and Xiangdong Wang[2,3]
[1]Department of Earth and Planetary Sciences, University of California–Davis, Davis, California 95616, USA
[2]Center for Excellence in Life and Paleoenvironment, Chinese Academy of Sciences, Nanjing 210008, China
[3]CAS Key Laboratory of Economic Stratigraphy and Palaeogeography, Nanjing Institute of Geology and Palaeontology, Chinese Academy of Sciences, Nanjing 210008, China
[4]State Key Laboratory of Palaeobiology and Stratigraphy, Nanjing Institute of Geology and Palaeontology, Chinese Academy of Sciences, Nanjing 210008, China

ABSTRACT

Earth's penultimate icehouse (ca. 340–285 Ma) was a time of low atmospheric pCO_2 and high pO_2, formation of the supercontinent Pangaea, dynamic glaciation in the Southern Hemisphere, and radiation of the oldest tropical rainforests. Although it has been long appreciated that these major tectonic, climatic, and biotic events left their signature on seawater $^{87}Sr/^{86}Sr$ through their influence on Sr fluxes to the ocean, the temporal resolution and precision of the late Paleozoic seawater $^{87}Sr/^{86}Sr$ record remain relatively low. Here we present a high-temporal-resolution and high-fidelity record of Carboniferous–early Permian seawater $^{87}Sr/^{86}Sr$ based on conodont bioapatite from an open-water carbonate slope succession in south China. The new data define a rate of long-term rise in $^{87}Sr/^{86}Sr$ (0.000035/m.y.) from ca. 334–318 Ma comparable to that of the middle to late Cenozoic. The onset of the rapid decline in $^{87}Sr/^{86}Sr$ (0.000043/m.y.), following a prolonged plateau (318–303 Ma), is constrained to ca. 303 Ma. A major decoupling of $^{87}Sr/^{86}Sr$ and pCO_2 during 303–297 Ma, coincident with the Paleozoic peak in pO_2, widespread low-latitude aridification, and demise of the pan-tropical wetland forests, suggests a major shift in the dominant influence on pCO_2 from continental weathering and organic carbon sequestration (as coals) on land to organic carbon burial in the ocean.

INTRODUCTION

Seawater $^{87}Sr/^{86}Sr$ has long been used as a tool for chronostratigraphic correlation (e.g., McArthur et al., 2012), and, in combination with global seawater $\delta^{13}C$, to constrain the timing and magnitude of tectonic events, continental weathering, and paleoclimate change (e.g., Kump and Arthur, 1997; Goddéris et al., 2017). For the middle to late Cenozoic, the high-resolution seawater $^{87}Sr/^{86}Sr$ curve has provided robust chronostratigraphic constraints and insight into the interlinked processes of the Earth system during our modern icehouse (e.g., Zachos et al., 1999).

The late Paleozoic ice age (LPIA, ca. 340–285 Ma) is one of two major icehouses of the Phanerozoic, and records the only greenhouse gas–forced transition from an icehouse with complex terrestrial ecosystems to a fully greenhouse world (Montañez and Poulsen, 2013). The LPIA was a time of very low atmospheric pCO_2 (Montañez et al., 2016) and high pO_2 (Glasspool et al., 2015), dynamic glaciation on Gondwana (Isbell et al., 2012), global tectonic reconfiguration (Veevers, 2013), and the evolution and radiation of the oldest tropical rainforests (DiMichele, 2014). The fingerprints of these events should have been recorded in seawater $^{87}Sr/^{86}Sr$ given they collectively influenced continental weathering, and thus Sr flux to the late Paleozoic oceans. The existing Carboniferous–early Permian seawater $^{87}Sr/^{86}Sr$ record derived using calcitic brachiopods (Bruckschen et al., 1999; Korte et al., 2006) remains only moderately resolved, reflecting stratigraphic uncertainties, relatively low temporal resolution, and possible diagenetic alteration.

Here, we present a $^{87}Sr/^{86}Sr$ record of unprecedented temporal resolution (10^5 yr) for ~38 m.y. of the LPIA, built using conodont bioapatite from an open-water carbonate slope succession (Naqing, south China) of the eastern Paleo-Tethys Ocean (Fig. DR1 in the GSA Data Repository[1]). Our record refines the structure of the middle Mississippian to early Permian seawater $^{87}Sr/^{86}Sr$ curve and places more precise temporal constraints on the timing of major shifts and rates of change. Integrated conodont apatite $^{87}Sr/^{86}Sr$ and carbonate $\delta^{13}C$ records provide insight into the relative roles of orogenic uplift, pan-tropical aridification, and the evolution of the paleo-tropical wetland rainforests on continental weathering and atmospheric pCO_2 during Earth's penultimate icehouse.

GEOLOGIC SETTING AND METHODS

During the Carboniferous–Permian, the South China Block was a nearly isolated terrain located at the interface of the Paleo-Tethys Ocean (west) and Panthalassic Ocean (east) (Fig. DR1). The Carboniferous–Permian Naqing succession in the Guizhou Province consists of thin-bedded lime mudstones intercalated with intraclast-bearing bioclastic wackestones to packstones (Fig. 1), and contains abundant conodonts with complete evolutionary lineages (Qi et al., 2014). The succession records near-continuous, hemipelagic deposition on a carbonate slope episodically punctuated by turbidity currents and debris flows in the Qian-Gui Basin that defined an open-water seaway to the Paleo-Tethys Ocean (Buggisch et al., 2011; Chen et al., 2016).

Sr was isolated from conodonts (n = 99) and carbonates (n = 22), collected from the Naqing section, using Eichrom exchange resin (50–100 μm) in pipette-tip columns attached to a Watson Marlow 205U Peristaltic pump (detailed methods are provided in the Data Repository). The $^{87}Sr/^{86}Sr$ ratios were measured on a Nu Plasma HR (Nu032) multicollector–inductively coupled plasma–mass spectrometer (MC-ICPMS) at the University of California–Davis (USA). Analytical precision (2 standard deviations [SD] = ±0.000026) is based on repeated $^{87}Sr/^{86}Sr$ analysis of

*E-mail: jtchen@nigpas.ac.cn

[1]GSA Data Repository item 2018128, analytical methods, age calibration, revision of pCO_2 estimates, Figures DR1 and DR2, and Tables DR1 and DR2, is available online at http://www.geosociety.org/datarepository/2018/, or on request from editing@geosociety.org.

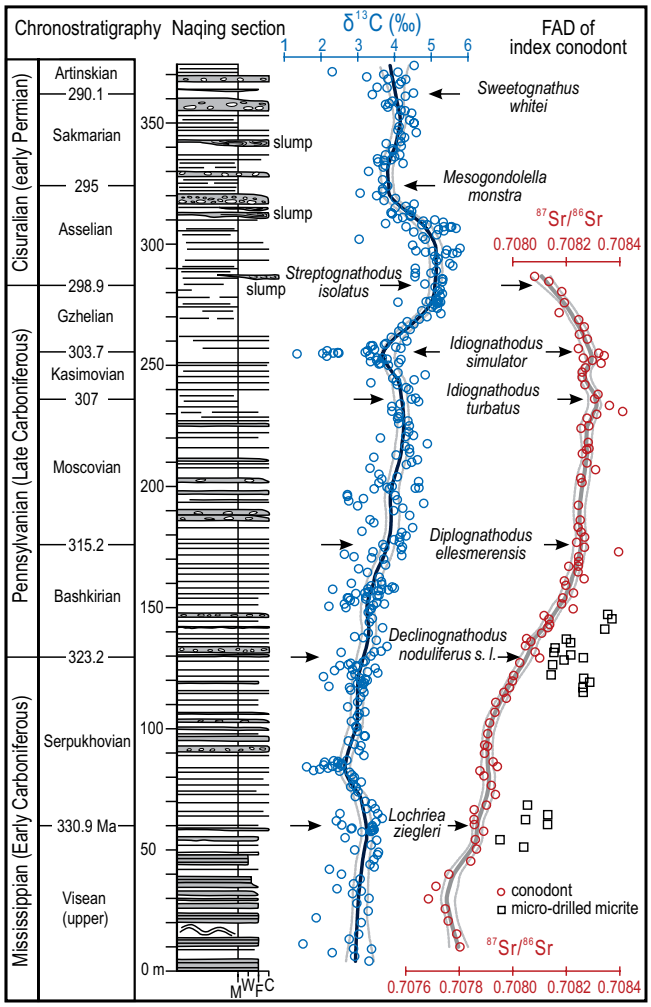

Figure 1. Conodont and carbonate $^{87}Sr/^{86}Sr$ (this study) and carbonate $\delta^{13}C$ (Buggisch et al., 2011) from the Naqing section, south China, with updated conodont biostratigraphy. Trend lines are locally weighted scatterplot smoothing (LOESS, 0.1 smoothing) regressions with 2.5% and 97.5% bootstrapped errors. M—lime mudstone; W—wackestone; F—fine-grained packstone; C—coarse-grained packstone; FAD—first appearance datum for conodont taxa.

strontium carbonate isotopic standard SRM 987 (avg. of 0.710251; n = 44) over the study period. All data are normalized to a SRM 987 value of 0.710249.

RESULTS AND DISCUSSION

Refined Seawater $^{87}Sr/^{86}Sr$

Conodont apatite $^{87}Sr/^{86}Sr$ values from the Naqing section delineate three phases during the middle Mississippian to early Permian (Fig. 1; Fig. DR2). First, after a brief decline from 0.70780 to 0.70769 during the Middle Mississippian (ca. 336–334 Ma), $^{87}Sr/^{86}Sr$ values increase rapidly (avg. of 0.000035/m.y.) over a 16 m.y. period (334–318 Ma) to 0.70827. Second, the $^{87}Sr/^{86}Sr$ values define an ~15 m.y. plateau throughout much of the Pennsylvanian (318–303 Ma). Third, $^{87}Sr/^{86}Sr$ values decline, at an average rate of 0.000043/m.y., from ca. 303 Ma through to the end of the record in the early Permian (ca. 298 Ma).

The $^{87}Sr/^{86}Sr$ values of diagenetically screened micrite from the Naqing section are overall higher, by up to 0.00029, than co-existing conodonts and exhibit greater scatter (Fig. 1). The Naqing conodont $^{87}Sr/^{86}Sr$ record largely agrees with a published first-order $^{87}Sr/^{86}Sr$ trend (Bruckschen et al., 1999; Korte et al., 2006), but with significantly less scatter and greater continuity (Fig. 2B). The Naqing data, with minimal stratigraphic uncertainty and higher temporal resolution (10^5 yr), refine the trend and fill in existing gaps. Notably, the Naqing $^{87}Sr/^{86}Sr$ values are comparable, within analytical uncertainty, with those of brachiopods from Panthalassic open-ocean settings (Brand et al., 2009) and of conodonts from the high-precision U-Pb calibrated Russian succession (Henderson et al., 2012).

Seawater $^{87}Sr/^{86}Sr$ represents a mixture of two main sources: a continent-derived, more-radiogenic weathering flux, and mantle-derived, less-radiogenic volcanic and hydrothermal fluxes. The rise in $^{87}Sr/^{86}Sr$ during ca. 334–318 Ma likely records the increased $^{87}Sr/^{86}Sr$ ratio of the riverine flux due to exposure and weathering of uplifted radiogenic basement rocks (Goddéris et al., 2017) driven by the Hercynian orogeny (ca. 340–260 Ma; Hatcher, 2002; Veevers, 2013). The subsequent protracted (15 m.y.) $^{87}Sr/^{86}Sr$ plateau (318–303 Ma) is interpreted to record sustained high-$^{87}Sr/^{86}Sr$ riverine flux due to westward progression of maximum elevations and subsequent rapid denudation of the highlands in the paleo-tropics. The new $^{87}Sr/^{86}Sr$ record indicates a rate of rise comparable to that of last 34 m.y. of the Cenozoic icehouse (0.000040/m.y.; McArthur et al., 2012, and references therein), suggesting that increased global weatherability due to orogenic uplift may be a common driver of these icehouses (cf. Kump and Arthur, 1997).

Conversely, the rapid, near-linear decline in $^{87}Sr/^{86}Sr$ ca. 303–285 Ma likely records decreased continental (silicate) weathering. This raises a paradox, as the potential for tectonically driven weatherability most likely remained unchanged through the early Permian (cf. Goddéris et al., 2017) with continued orogenesis to ca. 260 Ma (Hatcher, 2002). We hypothesize that continental weathering likely decreased during this time based on two other factors. First, the onset of widespread aridification in pan-tropical regions that began in the late Moscovian and intensified with time eastward across Pangaea through to the early Permian (Tabor and Poulsen, 2008; Michel et al., 2015) would have dramatically decreased silicate weathering. Second, the Euramerican tropical wetland forests underwent permanent turnover toward the close of the Carboniferous to dryland forests with less weathering potential (Wilson et al., 2017). Moreover, weathering of less-radiogenic basaltic provinces, which were emplaced initially in the latest Carboniferous and throughout the early Permian opening of the Neo-Tethys (e.g., Liao et al., 2015), may have contributed to declining $^{87}Sr/^{86}Sr$. The relative contribution of basalt weathering on global seawater $^{87}Sr/^{86}Sr$, however, was likely small in the latest Carboniferous–earliest Permian, as early basaltic province emplacement was limited in volume and occurred primarily in mid-latitude regions (Liao et al., 2015) where weathering rates would have been lower, in particular during the earliest Permian apex of glaciation.

Coupled $^{87}Sr/^{86}Sr$ and $\delta^{13}C$ and Implications for the Evolution of pCO_2 and pO_2

In order to evaluate the relative roles of silicate weathering and organic carbon (C_{org}) burial in regulating pCO_2, we couple the $^{87}Sr/^{86}Sr$ and carbonate $\delta^{13}C$ records and compare them to proxy-based pCO_2 estimates (Fig. 2). We present a consensus seawater $\delta^{13}C$ curve for the late Paleozoic (Fig. 2C) developed using published values of diagenetically screened brachiopods from Euramerican epeiric platforms (Grossman et al., 2008) and slope carbonates, argued to be unaltered by meteoric diagenesis (Buggisch et al., 2011).

Integrated isotopic records and published pCO_2 estimates delineate four intervals (Fig. 2). First, the long-term rise (ca. 334–318 Ma) and earlier portion of the $^{87}Sr/^{86}Sr$ plateau (318–309 Ma) correspond to a long-term decline in pCO_2 (~1200 to ~500 ppm) and to relatively stable $\delta^{13}C$ values (~3‰) between 340 Ma and 324 Ma, followed by a subsequent rise to a $\delta^{13}C$ maximum (>5‰) at ca. 309 Ma. Second, the later portion of the $^{87}Sr/^{86}Sr$ plateau (309–303 Ma) corresponds to a decline in $\delta^{13}C$ to its nadir (<3‰) at ca. 304 Ma and overall low pCO_2 values (~500–200 ppm), with a short-lived rise in pCO_2 at the end of the $^{87}Sr/^{86}Sr$ plateau.

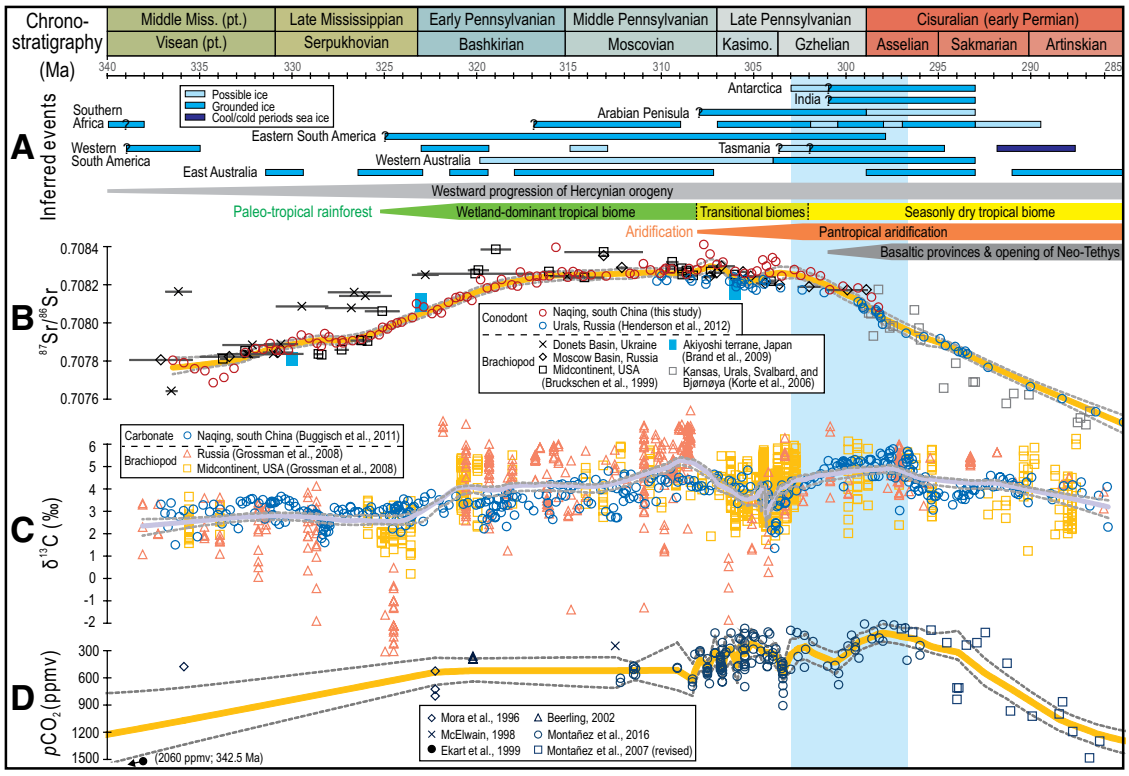

Figure 2. Inferred geologic events and proxy records for the late Paleozoic ice age (LPIA). A: Inferred geologic events (see text for explanation and references). (Glaciation history after Montañez and Poulsen [2013]; vegetation record modified from Montañez [2016]). B: Conodont-based $^{87}Sr/^{86}Sr$ record from Naqing, south China (this study) and the Urals, Russia (Henderson et al. 2012); previously published brachiopod ("good" data only) $^{87}Sr/^{86}Sr$ values renormalized to 0.710249 (strontium carbonate isotopic standard SRM 987). Locally weighted scatterplot smoothing (LOESS) trend lines for B (conodont-based $^{87}Sr/^{86}Sr$ values), C, and D are as in Figure 1. C: Age-recalibrated carbonate $\delta^{13}C$ record from Naqing and previously published brachiopod $\delta^{13}C$ records. D: Published atmospheric pCO_2 estimates (see the Data Repository [see footnote 1] for details). Vertical shading highlights interval of pCO_2 and $^{87}Sr/^{86}Sr$ decoupling.

Third, a decline in $^{87}Sr/^{86}Sr$ from 303 to 297 Ma is coincident with a renewed rise in $\delta^{13}C$ to ~5‰ and a drop in pCO_2 to its nadir (≤200 ppm). Fourth, continued decline in $^{87}Sr/^{86}Sr$ from 297 to 285 Ma corresponds to a decrease in $\delta^{13}C$ and a long-term rise in pCO_2.

Perturbations in global carbon cycling and atmospheric pCO_2 are thought to have been the primary driver of the initiation and demise of the LPIA (e.g., Montañez et al., 2007, 2016; Goddéris et al., 2017). Increased tectonically driven weatherability of silicate rocks inferred from the long-term rise in $^{87}Sr/^{86}Sr$ would have drawn down pCO_2 and initiated major glaciation (Goddéris et al., 2017). Radiation of the tropical forests in the latest Mississippian to their apex in the Middle Pennsylvanian (Fig. 2A; Cleal and Thomas, 2005; DiMichele, 2014) would have further contributed to lowering pCO_2 through enhanced silicate weathering and C_{org} sequestration in tropical wetlands (Nelsen et al., 2016). Evidence for this exists in the long-term $\delta^{13}C$ rise (Fig. 2C) and overall falling pCO_2 (Fig. 2D) through the Early and Middle Pennsylvanian. Major contraction of the Carboniferous tropical wetland rainforests during the Late Pennsylvanian (Kasimovian; Fig. 2A), however, would have decreased the terrestrial C_{org} sink (Cleal and Thomas, 2005; Montañez et al., 2016) as recorded in the widespread loss of coals, decreased $\delta^{13}C$ values (Fig. 2C), and increased pCO_2 (Fig. 2D).

While the coupled $^{87}Sr/^{86}Sr$ and $\delta^{13}C$ records provide support for the collective influence of orogenic uplift and expansion of the terrestrial tropical ecosystems on both accelerated weathering and overall decreasing pCO_2 through the Pennsylvanian, the records also reveal a paradoxical relationship with regard to the driver of the pCO_2 minimum across the Carboniferous–Permian transition. That is, reduced continental weathering driven by the aforementioned climatic and biotic factors and coincident with the rapid decline in $^{87}Sr/^{86}Sr$ between 303 Ma and 297 Ma hypothetically should have led to decreased consumption of atmospheric CO_2 and a consequent rise in pCO_2 (Goddéris et al., 2017). However, the proxy-based pCO_2 estimates decrease to a nadir across the Carboniferous–Permian transition (Fig. 2). While the low pCO_2 is consistent with the apex of late Paleozoic glaciation (Fig. 2A; Fielding et al., 2008; Isbell et al., 2012; Montañez and Poulsen, 2013) and eustatic fall of ~120 m (Rygel et al., 2008), it requires an additional driver given the aforementioned hypothesized decrease in continental weathering rates at this time.

One mechanism that could account for the pCO_2 minima coincident with peak pO_2 in the earliest Permian (Glasspool et al., 2015) is an increase in the magnitude of the C_{org} burial flux, which is supported by a return to more positive carbonate $\delta^{13}C$ values (Fig. 2C). An increase in terrestrial C_{org} burial rates is precluded by the loss of wetland forests and peat burial throughout Euramerica in the Late Pennsylvanian (Nelsen et al., 2016). We hypothesize that a major shift in the predominant C_{org} sink from land to the oceans occurred across the Carboniferous–Permian transition. Reconstructed paleo-plant physiology and process-based ecosystem modeling support this hypothesis and suggest a 2- to 6-fold increase in water-use efficiencies (WUE) of early Permian tropical plants relative to the Carboniferous wetland floral dominants (Wilson et al., 2017). This shift in WUE suggests an up to 50% decrease in canopy transpiration and a similar magnitude increase in surface runoff. Increased surface runoff would have resulted in greater delivery of nutrients and organic matter to coastal waterways, increasing the potential for increased primary productivity and C_{org} burial in the oceans. This hypothesized shift in the loci of late Paleozoic C_{org} burial sinks requires further evaluation through integrated biogeochemical and ecosystem modeling. It is further possible that hypothesized enhanced eolian delivery of reactive iron during the apex of the LPIA (Sur et al., 2015) would have further stimulated marine primary productivity and increased marine C_{org} burial.

In summary, coupled conodont apatite $^{87}Sr/^{86}Sr$ and carbonate $\delta^{13}C$ records indicate predominant roles for both continental weathering and C_{org} burial in regulating LPIA climate. A decoupling of pCO_2 from continental weathering across the Carboniferous–Permian transition (303–297 Ma), however, suggests that the coincident pCO_2 minimum and pO_2 maximum during the earliest Permian apex glaciation may record a previously unrecognized unidirectional shift in the primary loci of C_{org} burial from

land to sea. This shift was not a response to tectonically driven changes in weathering intensity or source, but rather to pantropical climate change and major ecosystem restructuring.

ACKNOWLEDGMENTS

We thank Q. Wang for picking conodont elements for Sr isotope analysis, and J. Glessner for assistance in Sr isotope analysis. We are grateful to J. Parrish for editorial handling of the manuscript and to E. Nardin, G. Gianniny, and A. Sedlacek for their constructive reviews. This work was supported by the Chinese Academy of Sciences (grants XDB18030400 and XDPB05), the National Natural Science Foundation of China (grants 41630101, 41290260, and 41672101), and U.S. National Science Foundation funding to Montañez (grant EAR1338281).

REFERENCES CITED

Beerling, D.J., 2002, Low atmospheric CO_2 levels during the Permo-Carboniferous glaciation inferred from fossil lycopsids: Proceedings of the National Academy of Sciences of the United States of America, v. 99, p. 12567–12571, https://doi.org/10.1073/pnas.202304999.

Brand, U., Tazawa, J.-i., Sano, H., Azmy, K., and Lee, X., 2009, Is mid-late Paleozoic ocean-water chemistry coupled with epeiric seawater isotope records?: Geology, v. 37, p. 823–826, https://doi.org/10.1130/G30038A.1.

Bruckschen, P., Oesmann, S., and Veizer, J., 1999, Isotope stratigraphy of the European Carboniferous: Proxy signals for ocean chemistry, climate and tectonics: Chemical Geology, v. 161, p. 127–163, https://doi.org/10.1016/S0009-2541(99)00084-4.

Buggisch, W., Wang, X., Alekseev, A.S., and Joachimski, M.M., 2011, Carboniferous–Permian carbon isotope stratigraphy of successions from China (Yangtze platform), USA (Kansas) and Russia (Moscow Basin and Urals): Palaeogeography, Palaeoclimatology, Palaeoecology, v. 301, p. 18–38, https://doi.org/10.1016/j.palaeo.2010.12.015.

Chen, J., Montañez, I.P., Qi, Y., Wang, X., Wang, Q., and Lin, W., 2016, Coupled sedimentary and $\delta^{13}C$ records of late Mississippian platform-to-slope successions from South China: Insight into $\delta^{13}C$ chemostratigraphy: Palaeogeography, Palaeoclimatology, Palaeoecology, v. 448, p. 162–178, https://doi.org/10.1016/j.palaeo.2015.10.051.

Cleal, C.J., and Thomas, B.A., 2005, Palaeozoic tropical rainforests and their effect on global climates: is the past the key to the present?: Geobiology, v. 3, p. 13–31, https://doi.org/10.1111/j.1472-4669.2005.00043.x.

DiMichele, W.A., 2014, Wetland-dryland vegetational dynamics in the Pennsylvanian Ice Age Tropics: International Journal of Plant Sciences, v. 175, p. 123–164, https://doi.org/10.1086/675235.

Ekart, D.D., Cerling, T.E., Montanez, I.P., and Tabo, N.J., 1999, A 400 million year carbon isotope record of pedogenic carbonate: Implications for paleoatmospheric carbon dioxide: American Journal of Science, v. 299, p. 805–827, https://doi.org/10.2475/ajs.299.10.805.

Fielding, C.R., Frank, T.D., Birgenheier, L.P., Rygel, M.C., and Jones, A.T., 2008, Stratigraphic imprint of the Late Paleozoic Ice Age in eastern Australia: A record of alternating glacial and nonglacial climate regime: Journal of the Geological Society, v. 165, p. 129–140, https://doi.org/10.1144/0016-76492007-036.

Glasspool, I.J., Scott, A.C., Waltham, D., Pronina, N., and Shao, L., 2015, The impact of fire on the Late Paleozoic Earth system: Frontiers in Plant Science, v. 6, p. 756, https://doi.org/10.3389/fpls.2015.00756.

Goddéris, Y., Donnadieu, Y., Carretier, S., Aretz, M., Dera, G., Macouin, M., and Regard, V., 2017, Onset and ending of the late Palaeozoic ice age triggered by tectonically paced rock weathering: Nature Geoscience, v. 10, p. 382–386, https://doi.org/10.1038/ngeo2931.

Grossman, E.L., Yancey, T.E., Jones, T.E., Bruckschen, P., Chuvashov, B., Mazzullo, S.J., and Mii, H.-s., 2008, Glaciation, aridification, and carbon sequestration in the Permo-Carboniferous: The isotopic record from low latitudes: Palaeogeography, Palaeoclimatology, Palaeoecology, v. 268, p. 222–233, https://doi.org/10.1016/j.palaeo.2008.03.053.

Hatcher, R.D., 2002, Alleghanian (Appalachian) orogeny, a product of zipper tectonics: Rotational transpressive continent-continent collision and closing of ancient oceans along irregular margins, *in* Martinez Catalán, J.R., et al., eds., Variscan-Appalachian Dynamics: The Building of the Late Paleozoic Basement: Geological Society of America Special Papers, v. 364, p. 199–208, https://doi.org/10.1130/0-8137-2364-7.199.

Henderson, C.M., Wardlaw, B.R., Vladimir, I.D., Schmitz, M.D., Schiappa, T.A., Tierney, K.E., and Shen, S., 2012, Proposal for base-Kungurian GSSP: Permophiles, v. 56, p. 8–21.

Isbell, J.L., Henry, L.C., Gulbranson, E.L., Limarino, C.O., Fraiser, M.L., Koch, Z.J., Ciccioli, P.L., and Dineen, A.A., 2012, Glacial paradoxes during the late Paleozoic ice age: Evaluating the equilibrium line altitude as a control on glaciation: Gondwana Research, v. 22, p. 1–19, https://doi.org/10.1016/j.gr.2011.11.005.

Korte, C., Jasper, T., Kozur, H.W., and Veizer, J., 2006, $^{87}Sr/^{86}Sr$ record of Permian seawater: Palaeogeography, Palaeoclimatology, Palaeoecology, v. 240, p. 89–107, https://doi.org/10.1016/j.palaeo.2006.03.047.

Kump, L.R., and Arthur, M.A., 1997, Global chemical erosion during the Cenozoic: weatherability balances the budgets, *in* Ruddiman, W.F., ed., Tectonic Uplift and Climate Change: New York, Springer, p. 399–426, https://doi.org/10.1007/978-1-4615-5935-1_18.

Liao, S.-Y., Wang, D.-B., Tang, Y., Yin, F.-G., Cao, S.-N., Wang, L.-Q., Wang, B.-D., and Sun, Z.-M., 2015, Late Paleozoic Woniusi basaltic province from Sibumasu terrane: Implications for the breakup of eastern Gondwana's northern margin: Geological Society of America Bulletin, v. 127, p. 1313–1330, https://doi.org/10.1130/B31210.1.

McArthur, J.M., Howarth, R.J., and Shields, G.A., 2012, Strontium Isotope Stratigraphy, *in* Gradstein, F., et al., eds., The Geologic Time Scale 2012: London, Elsevier, p. 127–144, doi: https://doi.org/10.1016/B978-0-444-59425-9.00007-X.

McElwain, J.C., 1998, Do fossil plants signal palaeoatmospheric carbon dioxide concentration in the geological past?: Philosophical Transactions of the Royal Society of London: Series B, Biological Sciences, v. 353, p. 83–96, https://doi.org/10.1098/rstb.1998.0193.

Michel, L.A., Tabor, N.J., Montañez, I.P., Schmitz, M.D., and Davydov, V.I., 2015, Chronostratigraphy and paleoclimatology of the Lodève Basin, France: Evidence for a pan-tropical aridification event across the Carboniferous–Permian boundary: Palaeogeography, Palaeoclimatology, Palaeoecology, v. 430, p. 118–131, https://doi.org/10.1016/j.palaeo.2015.03.020.

Montañez, I.P., 2016, A Late Paleozoic climate window of opportunity: Proceedings of the National Academy of Sciences of the United States of America, v. 113, p. 2334–2336, https://doi.org/10.1073/pnas.1600236113.

Montañez, I.P., and Poulsen, C.J., 2013, The Late Paleozoic ice age: An evolving paradigm: Annual Review of Earth and Planetary Sciences, v. 41, p. 629–656, https://doi.org/10.1146/annurev.earth.031208.100118.

Montañez, I.P., McElwain, J.C., Poulsen, C.J., White, J.D., DiMichele, W.A., Wilson, J.P., Griggs, G., and Hren, M.T., 2016, Climate, pCO_2 and terrestrial carbon cycle linkages during late Palaeozoic glacial–interglacial cycles: Nature Geoscience, v. 9, p. 824–828, https://doi.org/10.1038/ngeo2822.

Montañez, I.P., Tabor, N.J., Niemeier, D., DiMichele, W.A., Frank, T.D., Fielding, C.R., Isbell, J.L., Birgenheier, L.P., and Rygel, M.C., 2007, CO_2-forced climate and vegetation instability during Late Paleozoic deglaciation: Science, v. 315, p. 87–91, https://doi.org/10.1126/science.1134207.

Mora, C.I., Driese, S.G., and Colarusso, L.A., 1996, Middle to Late Paleozoic atmospheric CO_2 levels from soil carbonate and organic matter: Science, v. 271, p. 1105–1107, https://doi.org/10.1126/science.271.5252.1105.

Nelsen, M.P., DiMichele, W.A., Peters, S.E., and Boyce, C.K., 2016, Delayed fungal evolution did not cause the Paleozoic peak in coal production: Proceedings of the National Academy of Sciences of the United States of America, v. 113, p. 2442–2447, https://doi.org/10.1073/pnas.1517943113.

Qi, Y., Nemyrovska, T.I., Wang, X., Chen, J., Wang, Z., Lane, H.R., Richards, B.C., Hu, K., and Wang, Q., 2014, Late Visean–early Serpukhovian conodont succession at the Naqing (Nashui) section in Guizhou, South China: Geological Magazine, v. 151, p. 254–268, https://doi.org/10.1017/S001675681300071X.

Rygel, M.C., Fielding, C.R., Frank, T.D., and Birgenheier, L.P., 2008, The magnitude of Late Paleozoic glacioeustatic fluctuations: A synthesis: Journal of Sedimentary Research, v. 78, p. 500–511, https://doi.org/10.2110/jsr.2008.058.

Sur, S., Owens, J.D., Soreghan, G.S., Lyons, T.W., Raiswell, R., Heavens, N.G., and Mahowald, N.M., 2015, Extreme eolian delivery of reactive iron to late Paleozoic icehouse seas: Geology, v. 43, p. 1099–1102, 10.1130/G37226.1.

Tabor, N.J., and Poulsen, C.J., 2008, Palaeoclimate across the Late Pennsylvanian–Early Permian tropical palaeolatitudes: A review of climate indicators, their distribution, and relation to palaeophysiographic climate factors: Palaeogeography, Palaeoclimatology, Palaeoecology, v. 268, p. 293–310, https://doi.org/10.1016/j.palaeo.2008.03.052.

Veevers, J.J., 2013, Pangea: Geochronological correlation of successive environmental and strati-tectonic phases in Europe and Australia: Earth-Science Reviews, v. 127, p. 48–95, https://doi.org/10.1016/j.earscirev.2013.09.001.

Wilson, J.P., Montañez, I.P., White, J.D., DiMichele, W.A., McElwain, J.C., Poulsen, C.J., and Hren, M.T., 2017, Dynamic Carboniferous tropical forests: New views of plant function and potential for physiological forcing of climate: The New Phytologist, v. 215, p. 1333–1353, https://doi.org/10.1111/nph.14700.

Zachos, J.C., Opdyke, B.N., Quinn, T.M., Jones, C.E., and Halliday, A.N., 1999, Early cenozoic glaciation, antarctic weathering, and seawater $^{87}Sr/^{86}Sr$: Is there a link?: Chemical Geology, v. 161, p. 165–180, https://doi.org/10.1016/S0009-2541(99)00085-6.

Manuscript received 30 September 2017
Revised manuscript received 23 January 2018
Manuscript accepted 31 January 2018

Printed in USA